Quantitative Proteomics Reveals Dynamic Changes in the Plasma Membrane During *Arabidopsis* Immune Signaling*[S]

James Mitch Elmore‡§¶, Jun Liu‡§, Barrett Smith‡‖, Brett Phinney‡‖, and Gitta Coaker‡§**

The plant plasma membrane is a crucial mediator of the interaction between plants and microbes. Understanding how the plasma membrane proteome responds to diverse immune signaling events will lead to a greater understanding of plant immunity and uncover novel targets for crop improvement. Here we report the results from a large scale quantitative proteomics study of plasma membrane-enriched fractions upon activation of the *Arabidopsis thaliana* immune receptor RPS2. More than 2300 proteins were identified in total, with 1353 proteins reproducibly identified across multiple replications. Label-free spectral counting was employed to quantify the relative protein abundance between different treatment samples. Over 20% of up-regulated proteins have known roles in plant immune responses. Significantly changing proteins include those involved in calcium and lipid signaling, membrane transport, primary and secondary metabolism, protein phosphorylation, redox homeostasis, and vesicle trafficking. A subset of differentially regulated proteins was independently validated during bacterial infection. This study presents the largest quantitative proteomics data set of plant immunity to date and provides a framework for understanding global plasma membrane proteome dynamics during plant immune responses. ***Molecular & Cellular Proteomics 11: 10.1074/mcp.M111.014555, 1–13, 2012.***

Because many classes of plant pathogens remain outside the host cell membrane during infection, the plant plasma membrane (PM)[1] controls numerous facets of plant-microbe interactions. Initial pathogen recognition, signal transduction, and many downstream defense responses occur at the PM (1). Multiple immune receptors and signaling proteins localize to the PM as integral or peripheral proteins (1, 2). Understanding how diverse signals are translated into physiological changes at the PM will significantly enhance our knowledge of plant immune signaling and uncover novel proteins involved in plant defense at the cell membrane.

Plants rely on immune receptors at the cell surface or inside the cell to recognize invading microbial pathogens. PM-localized pattern recognition receptors recognize conserved microbial features, termed pathogen-associated molecular pattern (PAMP) or self-derived damage-associated molecular pattern (DAMP) molecules that are released during pathogen invasion and growth in the extracellular space (2). PAMP or DAMP recognition rapidly activates signaling networks that are propagated within the cell, modulating cellular physiology and ultimately resulting in changes in expression of defense-associated genes, which contribute to an effective immune response (2). These pattern-triggered immune (PTI) responses are thought to render most plants resistant to most non-adapted pathogens (2). However, host-adapted pathogens have developed virulence mechanisms to suppress PTI signaling and disable plant immune responses (1). Effector proteins represent one important class of these pathogen-derived virulence factors. Pathogen effectors primarily function inside host cells where they modify host proteins and/or processes to evade or disable plant immunity (3).

Plants also use intracellular immune receptors to monitor for effector-induced changes. Effector recognition is mediated by primarily intracellular resistance (R) proteins that commonly belong to the nucleotide-binding leucine-rich repeat (NB-LRR) family of proteins. R protein activation results in effector-triggered immunity (ETI) (1). R proteins can detect effectors either through direct binding or indirectly via host accessory proteins. The first accessory protein discovered was the peripheral PM protein RIN4 (RPM1-interacting protein 4), which can regulate plant immunity at multiple levels (4–8). RIN4 associates with two plant R proteins, RPM1 and RPS2, and is targeted by multiple bacterial effectors including AvrB, AvrRpm1, AvrRpt2,

From the ‡University of California at Davis, Davis, California 95616, the §Department of Plant Pathology, and the ‖Genome Center Proteomics Core Facility

Received September 20, 2011, and in revised form, November 11, 2011

Published, MCP Papers in Press, January 3, 2012, DOI 10.1074/mcp.M111.014555

[1] The abbreviations used are: PM, plasma membrane; ETI, effector-triggered immunity; HR, hypersensitive response; PAMP, pathogen-associated molecular pattern; PTI, pattern-triggered immunity; SpC, spectral count(s); DAMP, damage-associated molecular pattern; Dex, dexamethasone; FDR, false discovery rate; GO, Gene Ontology; HRP, horseradish peroxidase; SNARE, soluble *N*-ethylmaleimide-sensitive factor attachment protein receptor; SAM, *S*-adenosylmethionine; RLK, receptor-like kinase; NOI, nitrate-induced; CYP, cytochrome P450; WT, wild type.

and HopF2, all of which localize to the plant PM (4, 6, 9, 10). AvrB can induce phosphorylation of RIN4 through host receptor-like cytoplasmic kinases, a molecular event that is recognized by the RPM1 immune receptor (11, 12). AvrRpt2 is a protease that directly cleaves RIN4, and this event activates the RPS2 immune receptor, leading to ETI (5, 6). Although both ETI and PTI share similar signaling requirements and defense outputs, ETI induces a stronger response than PTI (13). ETI is often associated with a form of programmed cell death termed the hypersensitive response (HR) (13).

The model plant *Arabidopsis thaliana* has been instrumental in the genetic and molecular dissection of plant immune responses. Forward and reverse genetics, two-hybrid based screens, and proteomics studies have been useful for identifying immune receptors and deciphering molecular events following pathogen recognition, but many of the downstream events that lead to effective immunity are still unclear (1, 2, 14–17). Two-dimensional gel electrophoresis-based investigations into plant immune responses have been limited in scope because of restrictions in dynamic range and resolving power, with each study identifying less than 40 proteins as significantly changing (18–20). Recent cell culture-based quantitative LC-MS/MS proteomics studies have uncovered early plant immune signaling at the PM. Phosphoproteomic analyses of PM proteins following PAMP perception have uncovered post-translational modifications that contribute to activity of the reactive oxygen species-generating protein RBOHD and the PM H^+-ATPase AHA1, as well as residues that are differentially phosphorylated on other proteins involved in defense responses (14, 15). A proteomic examination of PAMP-induced changes in detergent-resistant membrane protein composition suggests that specific immune signaling proteins are rapidly recruited to PM microdomains during PTI signaling (16). These studies highlight the dynamic behavior of signaling proteins at the PM, but there have been no reports of global PM proteome changes during plant immune signaling.

In addition to early signaling events, it is expected that plant PM proteins mediate downstream immune responses that contribute to pathogen resistance. *Arabidopsis* mutants compromised in penetration resistance to nonadapted fungi are defective in proteins involved in PM transport and vesicle trafficking (21). A recent cytological study implicates a vacuole-PM fusion event during ETI that facilitates the extracellular discharge of antimicrobial and cell death-promoting vacuolar contents (22). Despite the importance of the PM in plant immune responses, the complement of PM proteins directly responsible for resistant plant phenotypes is largely unknown. A comprehensive understanding of dynamic changes in the PM proteome during pathogen recognition will significantly advance our understanding of plant immune signaling networks.

In this study, we used quantitative proteomics to investigate dynamic changes in PM-enriched fractions after activation of the plant immune receptor RPS2. Gel-enhanced LC-MS/MS was employed in combination with spectral counting to determine relative protein levels in control and treated samples. 1353 proteins were reproducibly identified in PM-enriched fractions across multiple treatment replicates. These quantitative proteomics results emphasize the importance of dynamic signaling events, primary and secondary metabolism, vesicle trafficking, and transport at the PM during plant immunity. A subset of proteins whose levels change differentially during immune responses was independently validated during bacterial infection. These results highlight the dynamic nature of the PM proteome during plant immune signaling.

EXPERIMENTAL PROCEDURES

Plant Material and Dexamethasone Treatment—All *Arabidopsis* plants were grown in soil in a controlled environment chamber at 24 °C with a 10-h light/14-h dark photoperiod under a light intensity of 85 $\mu E/m^2/s$. Dexamethasone (Dex)-inducible GVG-AvrRpt2 (23) transgenic plants in the Col-0 (RPS2) background were used to initiate ETI. GVG-AvrRpt2 plants were sprayed with 30 μM Dex in water containing 0.025% Silwett L-77 surfactant. Col-0 WT plants sprayed with 30 μM Dex containing 0.025% Silwett L-77 were used as a negative control. Plants were incubated on a light bench at 23 °C for 6 h before harvesting tissue for plasma membrane enrichment. Three biological replicates of plants grown and harvested at different times were performed. Four- to 5-week-old plants were used for all experiments.

Plasma Membrane Enrichment—Plasma membrane enrichment was performed using aqueous two-phase partitioning essentially as in Refs. 8 and 24. The final upper phase fraction containing enriched plasma membrane vesicles was incubated with 0.02% Brij-58 detergent on ice for 10 min to invert vesicles and release cytosolic contaminants (25). The samples were then diluted 20 times with H_2O and centrifuged at 90,000 $\times$ *g* for 60 min to pellet plasma membrane vesicles. The membrane pellets were frozen in liquid N_2 and stored at −80 °C.

Sample Preparation for MS—Membrane pellets were solubilized in 2$\times$ Laemmli buffer without bromphenol blue then delipidated using a chloroform-methanol-H_2O precipitation technique (26, 27). Precipitated proteins were solubilized in 2$\times$ Laemmli containing 6 M urea in a sonicating water bath. Protein samples were quantified using a RC DC protein assay (Bio-Rad). PM-enriched fractions (300 μg of total protein) from control and GVG-AvrRpt2 samples were subjected to one-dimensional SDS-PAGE using an 8–16% precise protein gradient gel (Thermo Scientific). The entire sample lane was excised and cut into 15 pieces of equal size using a disposable grid cutter (The Gel Company). In-gel digestions were performed with trypsin in a barocycler (Pressure Biosciences) according to Refs. 28 and 29. The digested peptides were dried using a vacuum concentrator and then solubilized in 120 μl of 2% acetonitrile, 0.1% trifluoroacetic acid for LC-MS/MS analysis.

LC-MS/MS—Separate LC-MS/MS analyses were performed on peptides derived from individual gel pieces for a total of 15 LC-MS/MS runs per sample. The LC-MS/MS system configuration consisted of a CTC Pal autosampler (LEAP Technologies) and Paradigm HPLC (Michrom BioResources) coupled to a LTQ ion trap mass spectrometer (Thermo Scientific) with a CaptiveSpray ionization source (Michrom BioResources). Reversed phase LC was performed by injecting 60 μl of each digested peptide sample onto a Zorbax300SB-C18 trap column (5 μm, 5 $\times$ 0.3 mm; Agilent Technologies) and desalted online. The peptides were then eluted from the trap and separated on a reverse phase Michrom Magic C18AQ (200 μm $\times$ 150 mm) capillary column at a flow rate of 2 μl/min using a 120-min gradient (2–35% buffer B 85 min, 35–80% buffer B 25 min,

2% buffer B 10 min; buffer A = 0.01% formic acid in H_2O, buffer B = 100% acetonitrile). The mass spectrometer was operated in data-dependent acquisition mode with 60-s dynamic exclusion enacted on *m/z* observed twice within 30 s. A standard Top10 acquisition method was used with one survey MS scan followed by MS/MS scans on the 10 most intense ions.

Protein Identifications—Tandem mass spectra were extracted using Bioworks 3.3 and analyzed using the X!Tandem GPM-XE Tornado version 2009.04.01.3 spectrum modeler (30) (http://www.thegpm.org). X!Tandem was configured to search the UniProtKB *Arabidopsis* complete proteome sequence database (downloaded July 7, 2010; 31,881 entries) and common repository of adventitious proteins database (version 1.0; 112 entries). A reversed and concatenated database served as a decoy sequence database to determine protein false discovery rate (FDR) as in Ref. 31. X!Tandem was configured to allow parent ion mass error of 1.8 Da and fragment mass error of 0.4 Da. The data were searched using complete carbamidomethyl modification of cysteine residues and potential modifications of oxidation of methionine and tryptophan, deamidation of asparagine and glutamine in round 1, and dioxidation of methionine and tryptophan in round 2 and allowing one missed cleavage. X!Tandem search results were imported into Scaffold 3.0.7 (Proteome Software), and all MS runs corresponding to the same sample were grouped together. Peptide identifications were modeled using the PeptideProphet algorithm (32). Protein identification FDR was determined empirically using hits from the reversed decoy database (31). Protein identifications required two unique peptides, a 50% peptide probability, and a 90% protein probability. Using these identification thresholds, the data set contained 380,651 spectra and 2385 proteins with 0.1% peptide FDR and 4.5% protein FDR (31, 32). The Scaffold protein report containing the protein identification probabilities, number of unique peptides, unique spectra, and total spectra is available in supplemental Table 4.

Shared Peptide Distribution and Quantitative Analysis—The Spectrum Report was exported from Scaffold 3. Nonunique (shared) peptide spectra were distributed among potential parent proteins based on distribution ratios derived from the unique spectral count of each protein as in Ref. 33 using a custom script developed at the University of California Davis Genome Center Bioinformatics core facility (34). All UniProt-KB database hits derived from the same *Arabidopsis* TAIR gene identifier (*i.e.* different gene models) were added and collapsed onto the TAIR ID to simplify data analysis. All of the Uniprot identifiers corresponding to each *Arabidopsis* TAIR gene identifier are listed in supplemental Table 5. For relative protein quantification between Col-0 and GVG-AvrRpt2 samples, the QSpec statistical framework (Version 2, http://sourceforge.net/projects/qspec/) was used to assign significance to differentially regulated proteins (35). Proteins were considered differentially regulated in QSpec if Bayes factor $>$ 10, FDR $<$ 0.01, and fold change $>$ $\pm$50% and if the proteins were identified in at least two replicates of a particular treatment with an average of at least five spectral counts per replicate.

Process Over-Representation Analysis—DAVID Bioinformatics Resources version 6.7 (36) was used to detect Gene Ontology (GO) Biological Process over-representation in the up- and down-regulated protein groups using all identified proteins as the background set. The DAVID Functional Annotation Clustering Tool was used to cluster enriched terms using a similarity threshold of 0.45. The most significant representative term from each cluster with $p < 0.1$ was reported.

Antibodies and Immunoblot Analysis—SDS-PAGE and immunoblotting were performed according to standard procedures. The following antibodies were used at the indicated concentrations: rabbit anti-RIN4 (1:1000) (8), rabbit anti-PMA2 (1:10,000) (37), rabbit anti-TOC75 (1:6000) (38), mouse anti-voltage-dependent anion channel (1:100) (PM035; Dr. T. Elthon, University of Nebraska, Lincoln, NE), goat anti-BIP (1:500) (Santa Cruz Biotechnology), rabbit anti-PED1 (1:1000) (39), chicken anti-αTIP (1:1000) (Dr. N. Raikhel, University of California, Riverside, CA), mouse anti-HSC70 (1:1000) (Enzo Life Sciences), rabbit anti-HSP90 (1:1500) (Agrisera), rabbit anti-TCH3 (1:2000) (40), rabbit anti-PLP2a (1:1000) (41), and rabbit anti-SYP122 (1:3000) (42). Secondary goat anti-rabbit IgG-HRP (Bio-Rad), goat anti-mouse IgG-HRP (Bio-Rad), bovine anti-goat IgG-HRP (Santa Cruz Biotechnology), or goat anti-chicken IgY-HRP (Santa Cruz Biotechnology) conjugates were used at a concentration of 1:3000 for detection using enhanced chemiluminescence (Pierce).

Immunoblot Image Analysis—X-ray film from immunoblotting was scanned using an office photo scanner set to grayscale at 300dpi and exported in .tif format. ImageJ (http://rsbweb.nih.gov/ij/) was used for densitometric analysis of all images as in Ref. 43. Signal bands were outlined, profile plots were generated, and the area under the curve was measured in arbitrary units. All three biological replicates used for LC-MS/MS analysis were simultaneously processed on the same protein immunoblot.

Bacterial Strains and Plant Inoculations—*Pseudomonas syringae* pv. *tomato* strain DC3000 (*Pst* DC3000) carrying the broad host range vector pVSP61 empty vector or pVSP61 AvrRpt2 (44) was vacuum-infiltrated on 4-week-old *Arabidopsis* plants at a concentration of 5×10^7 cfu/ml in 10 mM $MgCl_2$ containing 0.01% Silwett L-77 surfactant. The plants were incubated on a light bench for 15 h at 23 °C before harvesting tissue for plasma membrane enrichment. The experiments were performed three times with similar results.

RESULTS AND DISCUSSION

Plant Material and Proteomics Workflow—To activate plant ETI responses in the absence of the pathogen, 4-week-old Dex-inducible AvrRpt2 (GVG-AvrRpt2) transgenic *Arabidopsis* Col-0 lines were used (23). The Dex-inducible GVG system consists of a chimeric transcription factor (GVG) with a glucocorticoid-binding domain that activates transcription of target genes (*e.g.* AvrRpt2) upon application of Dex to the leaf surface. Activation of ETI in the absence of the pathogen mitigates confounding effects (*e.g.* PAMP perception, additional effectors, and toxins) that would be introduced using bacterial infection. GVG-AvrRpt2 plants appear phenotypically normal in the absence of Dex and have been previously shown to specifically accumulate *avrRpt2* transcript and protein only after Dex application (23). The bacterial effector AvrRpt2 is a protease that undergoes autoproteolysis, localizes to the PM, and cleaves the plant protein RIN4 twice at the sequence VP*x*FG*x*W, a molecular event that is recognized by the RPS2 resistance gene in the Col-0 background (5, 6, 45, 46). Activation of RPS2 initiates ETI signaling and culminates in a HR (full tissue collapse) 7–8 h post-Dex application (data not shown). RIN4 levels in Col-0 and GVG-AvrRpt2 plants were monitored by immunoblotting each hour following Dex application for 8 h (Fig. 1*B*). RIN4 protein levels decrease significantly between 5 and 6 h post-Dex treatment, and the 6-h time point was selected to harvest tissue for plasma membrane enrichment. The 6-h time point coincides with the initial loss of leaf turgor in GVG-AvrRpt2 plants (Fig. 1A). At this time point it is expected that other AvrRpt2 targets in addition to RIN4 would be cleaved from the PM and degraded.

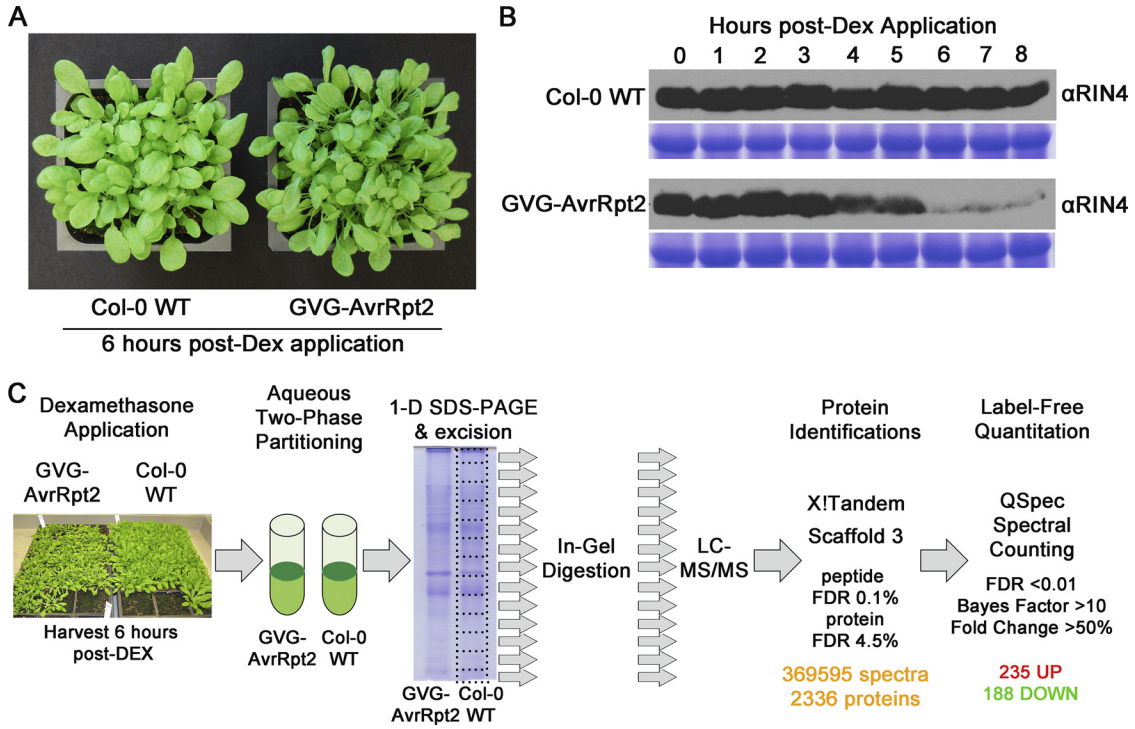

FIG. 1. **Plant material and experimental design.** *A*, Dex-inducible expression of AvrRpt2 activates ETI responses. Col-0 WT and GVG-AvrRpt2 plants were sprayed with 30 μM Dex + 0.025% Silwett L-77. Pictures were taken 6 h post-Dex treatment. *B*, AvrRpt2 induces RIN4 degradation by 6-h post-Dex treatment. Immunoblot analysis of RIN4 protein levels in Col-0 WT and GVG-AvrRpt2 plants. Coomassie staining indicates equal protein loading. *C*, schematic representation of proteomics workflow. PM vesicles were harvested 6 h post-Dex application and subjected to one-dimensional (*1-D*) SDS-PAGE, and the resulting gel lane was cut into 15 pieces. LC-MS/MS was performed on tryptic peptides from each gel slice, and results for each sample were combined for protein identifications and quantitative spectral counting analysis.

Our proteomics workflow is represented in Fig. 1*C*. Leaf rosette tissue was harvested from Col-0 and GVG-AvrRpt2 plants 6 h post-Dex application, and the total microsomal fraction was immediately subjected to aqueous two-phase partitioning to enrich for plasma membrane vesicles (24). The nonionic detergent Brij-58 was used to invert the isolated vesicles and release cytosolic protein contaminants (25). PM-enriched samples were quantified, and the samples were subjected to one-dimensional SDS-PAGE to fractionate proteins by size. Each gel lane was divided into 15 equal sections and processed individually, yielding 15 LC-MS/MS runs per sample. X!Tandem was used to search the UniprotKB complete *Arabidopsis* proteome database for protein identifications. All of the data from a single sample were then combined in Scaffold 3 (Proteome Software) for peptide and protein identification modeling. Peptide and protein identification FDR was limited to 0.1 and 4.5%, respectively (31, 32). The Spectrum Report was exported from Scaffold 3 and used to distribute shared peptide spectra as in Ref. 33 using a custom script (34), yielding a data set containing 369,595 spectra and 2336 proteins. Removal of common laboratory contaminants resulted in a total list of 2303 *Arabidopsis* proteins. The complete list of identified proteins, associated spectral counts (SpC), and quantitative statistics is available in supplemental Table 1.

Plasma Membrane Enrichment—Aqueous two-phase partitioning is a well established method for enrichment of plasma membrane vesicles from total cellular microsomal fractions (47). We evaluated the purity of PM-enriched fractions isolated in our laboratory by immunoblotting with antibodies raised against known subcellular membrane markers (Fig. 2*A*). When compared with total leaf and total microsomal fractions, the PM fraction was enriched in the integral PM H^+-ATPase and peripheral PM protein RIN4 (Fig. 2*A*). Furthermore, all other subcellular membrane markers were depleted in the PM-enriched fraction, indicating that PM vesicles of relatively high purity were obtained using the two-phase partitioning enrichment protocol (Fig. 2*A*).

Upon completion of LC-MS/MS and protein identifications, the subcellular location database for *Arabidopsis* proteins, SUBA (48), was used for *in silico* localization of all proteins identified in our experiments. SUBA was queried for all published experimental (*e.g.* GFP fusion protein microscopy, MS/MS, etc.) and predicted evidence of the subcellular location of a protein. All of the database hits (experimental, predicted, or experimental and predicted) for a given subcellular location are reported in Fig. 2*B*. Of the 2303 proteins identified, 63% (1453) have been previously shown or predicted to be associated with the plasma membrane. A previous study estimated that protein contamination from other subcellular com-

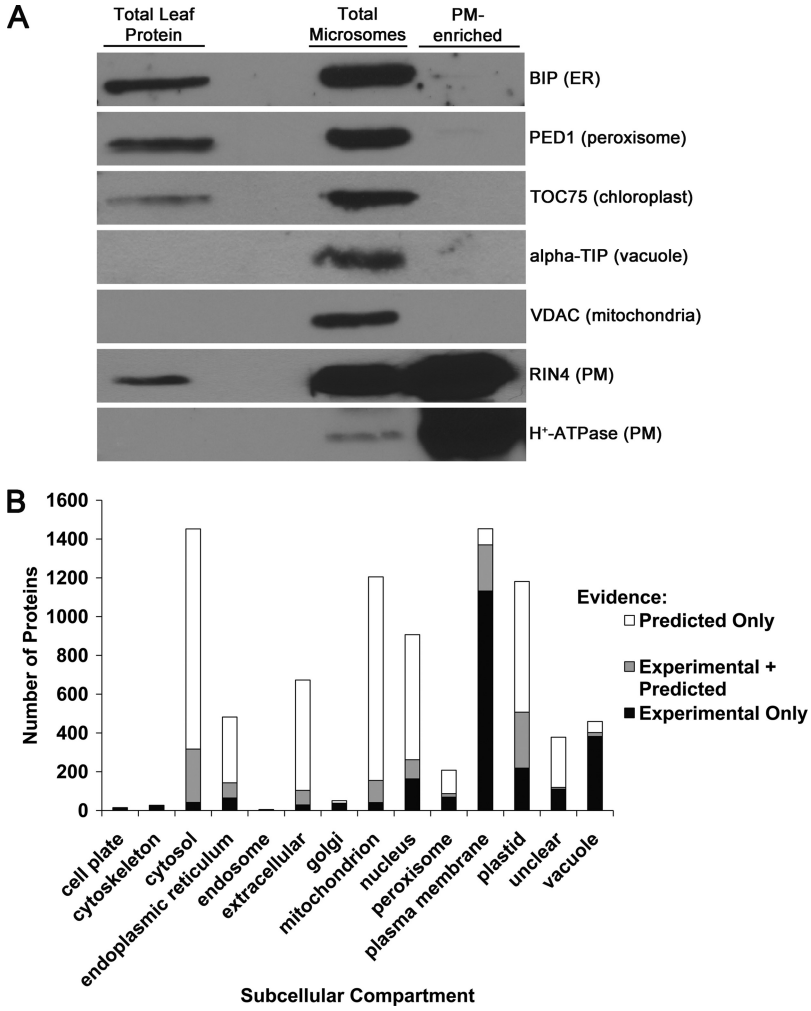

FIG. 2. **Plasma membrane enrichment.** *A*, immunoblot analysis of aqueous two-phase partitioning PM enrichment. Total leaf, total microsome, and PM-enriched fractions are probed with antibodies raised against the indicated proteins. Established protein subcellular localization is indicated within *parentheses*. *ER*, endoplasmic reticulum; *BIP*, luminal-binding protein 1; *PED1*, peroxisome defective 1; *TOC75*, translocon at the outer envelope membrane of chloroplast 75; *alpha-TIP*, tonoplast intrinsic protein α; *VDAC*, voltage-dependent anion channel; *RIN4*, RPM1-interacting protein 4. Ten μg of total protein was loaded per lane. *B*, *in silico* localization of all proteins identified by LC-MS/MS. The proteins were queried using the subcellular location database for *Arabidopsis* proteins (SUBA 2.21).

partments was as high as 26% after PM enrichment using two-phase partitioning followed by membrane stripping using $NaCO_3$ (49). Because no PM stripping protocol was employed, it is expected that our PM-enriched fractions contain proteins loosely associated with the PM. It is accepted that no organellar enrichment strategy can achieve 100% purity (49). However, the localization results show that our data set is highly enriched for plasma membrane proteins relative to other subcellular compartments.

Reproducibility of Spectral Count Data—Spectral counting has been widely adopted as a robust label-free approach to quantitative proteomics (50). SpC, defined as the total number of observations of a protein in a MS/MS experiment, are highly correlated with absolute protein abundance in complex samples over at least 2 orders of magnitude (51). We therefore used SpC as a relative protein abundance measure in our samples. Table I reports the pairwise Pearson correlations between all replicates of Col-0 WT and GVG-AvrRpt2 tissue samples. Examining the entire data set of all identified proteins, we found that pairwise Pearson correlation coefficients of normalized SpC between replicates within a treatment were high ($r = 0.88$–0.93) (Table I). Low abundance proteins, or those that are identified infrequently with low numbers of SpC, are common in MS/MS experiments with complex samples, and reports indicate that proteins identified with less than five SpC are difficult to reliably quantify (50). We therefore focused our attention on proteins that were reproducibly identified across two or more replicates of a biological condition (*i.e.* two replicates of treatment or two replicates of control) with an average of five SpC per replicate. 59% or 1353 of all identified proteins satisfied these criteria and were assigned to the set of reproducible protein identifications (supplemental Table 1). SUBA examination of this protein subset revealed that 75% of the reproducibly identified proteins have previous experimental or predicted evidence of PM localization (data not shown).

Supplemental Fig. 1 depicts the protein identification overlap across treatments and within treatment replicates for the entire data set and the reproducibly identified protein subset. As expected, proteins of higher abundance were more likely to be identified across multiple replicates, and most were identified in both Col-0 WT and GVG-AvrRpt2 samples (supplemental Fig. 1 and supplemental Table 1).

TABLE I
Linear Pearson correlation coefficients of protein spectral counts amongst replicates
SpC were normalized to total number of spectra in each replicate before analysis. Rep, replicate.

	Pairwise Pearson correlations for all proteins					
	Col-0 WT Rep 1	Col-0 WT Rep 2	Col-0 WT Rep 3	GVG-AvrRpt2 Rep 1	GVG-AvrRpt2 Rep 2	GVG-AvrRpt2 Rep 3
Col-0 WT Rep 1		0.9271	0.8812	0.9109	0.8623	0.8272
Col-0 WT Rep 2	0.9271		0.9311	0.8535	0.9143	0.847
Col-0 WT Rep 3	0.8812	0.9311		0.8223	0.8783	0.9159
GVG-AvrRpt2 Rep 1	0.9109	0.8535	0.8223		0.9017	0.8987
GVG-AvrRpt2 Rep 2	0.8623	0.9143	0.8783	0.9017		0.9095
GVG-AvrRpt2 Rep 3	0.8272	0.847	0.9159	0.8987	0.9095	

Relative Quantification—To assign significance to differentially regulated proteins, the QSpec statistical framework was used to model the SpC data set (35). QSpec uses a hierarchical Bayes generalized linear mixed effects model approach to model SpC, taking into account common variables associated with SpC such as nonparametric data distributions, adjustments for protein length and the total number of SpC in each sample replicate, variance associated with low SpC, and differential expression. QSpec assigns to each protein a significance factor (termed the Bayes factor), which is the ratio of the likelihood of the model with differential expression over the model without differential expression (35). Thus, higher Bayes factors indicate higher confidence that a given protein is differentially regulated. Bayes factor values in the data set ranged from 0.007 to 1.7×10^{16} (supplemental Table 1). Thresholds to determine protein differential regulation were selected as follows: Bayes factor > 10, FDR < 0.01, fold change $> \pm 50\%$, and reproducibly identified in two or more replicates of a biological condition with an average of five SpC. Additionally, proteins must exhibit $>50\%$ fold change in at least two biological replicates of a treatment to be considered differentially regulated. Lower confidence proteins (caused by low SpC, low fold change, or poor reproducibility) were filtered using these stringent criteria. Under these thresholds, 235 proteins were significantly up-regulated (supplemental Table 2), whereas 188 proteins were significantly down-regulated (supplemental Table 3).

Differentially Regulated Proteins and Biological Process Over-representation—To better understand the biological significance underlying differentially regulated proteins, biological process enrichment was performed using the DAVID Bioinformatics Resources annotation tool (http://david.abcc.ncifcrf.gov) (36). Results from functional annotation clustering of significantly enriched GO biological process terms in the up- and down-regulated protein sets are presented in Figs. 3 and 4, respectively. Process over-representation was determined relative to the background set of all identified proteins. We will highlight several processes/protein families that are enriched in significantly changing protein sets.

Up-regulated Proteins and Processes—The full list of significantly up-regulated proteins grouped by biological function is reported in supplemental Table 2. The most highly

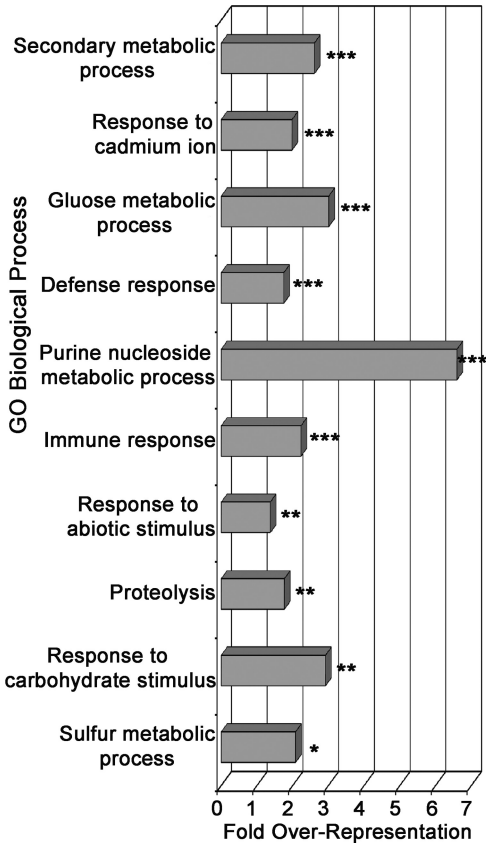

FIG. 3. **GO biological process over-representation in up-regulated proteins during ETI.** The *bar chart* represents fold enrichment of GO biological process terms in the up-regulated protein set relative to background set of all identified proteins. The DAVID Bioinformatics Resources functional annotation clustering algorithm was used to cluster similar terms. The most significant representative term in each cluster is reported. The terms are ordered from most significant (*top*) to least significant (*bottom*). ***, $p < 0.01$; **, $p < 0.05$; *, $p < 0.1$.

enriched up-regulated processes include cellular responses to cadmium, primary and secondary metabolism, immune responses, abiotic stress responses, and proteasome-mediated protein catabolism (Fig. 3 and supplemental Table 2). Cadmium is known to induce reactive oxygen species production in plant cells and can trigger cell death at high concentrations (52). The enrichment of cadmium-responsive gene products in the up-regulated protein set suggests that

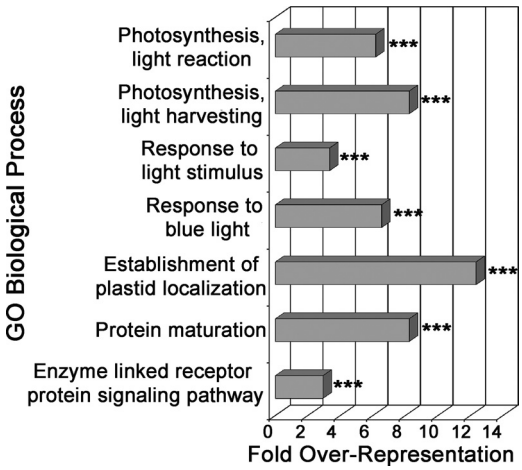

FIG. 4. **GO biological process over-representation in down-regulated proteins during ETI.** The *bar chart* represents fold enrichment of GO biological process terms in the down-regulated protein set relative to the background set of all identified proteins. The DAVID Bioinformatics Resources functional annotation clustering algorithm was used to cluster similar terms. The most significant representative term in each cluster is reported. The terms are ordered from most significant (*top*) to least significant (*bottom*). ***, $p < 0.01$; **, $p < 0.05$; *, $p < 0.1$.

similar cell death processes may be activated during onset of HR in response to ETI (Fig. 3). As others have observed, many enzymes involved in primary metabolism moderately increased during ETI, suggesting an increased demand for energy and carbon skeletons during execution of defense responses (Fig. 3 and supplemental Table 2) (19, 53). Many enzymes involved in the membrane transport of diverse molecules such as phospholipids, ions, sugars, and abscisic acid were also found to be up-regulated. A large proportion of up-regulated proteins (~22%) have previously characterized roles in plant immunity or cell death regulation, including those involved in calcium and lipid signaling, membrane transport, phosphorylation, chaperones, redox homeostasis, secondary metabolism, and membrane trafficking (supplemental Table 2).

Camalexin Biosynthesis—One of the secondary metabolic processes that was up-regulated during ETI was the production of camalexin, the major phytoalexin or induced antimicrobial compound of *Arabidopsis* (54). Enzymes catalyzing the final steps of camalexin biosynthesis, phytoalexin-deficient 3 (PAD3 or CYP71B15), CYP71A12, and CYP71A13, were identified as highly up-regulated (Fig. 3 and supplemental Table 2) (55–57). Protein levels of phytochelatin synthase 1 and glutathione *S*-transferase Phi 6, enzymes recently implicated in camalexin biosynthesis, were also increased (58) (supplemental Table 2). The subcellular localization of camalexin biosynthesis is currently unknown, and these data suggest that it could be a membrane-associated process. Camalexin inhibits the growth of many fungi (59). Camalexin biosynthesis during ETI may protect dying tissue from invasion by opportunistic necrotrophs, pathogens that derive nutrients from dead tissue. Antimicrobial production at the PM near sites of transport out of the cell is hypothesized to be a common mechanism of plant defense (21).

Lipid Signaling—Stress-induced lipid signaling has emerged as a key regulator of cellular responses to a variety of stimuli (60). Several proteins with distinct phospholipase activities were significantly up-regulated (supplemental Table 2). Phosphatidic acid, a critical lipid second messenger, has been shown to increase during activation of ETI and contribute to defense gene induction and cell death (61). It was proposed that phosphatidic acid accumulation during ETI was biphasic with an initial phase dependent on the concerted activities of phospholipase C/diacylglerol kinase and a later phase dependent on phospholipase D activity (61). PLC1 and PLC2 levels did not change significantly, although diacylglycerol kinase 5 was up-regulated (supplemental Tables 1 and 2). However, we identified two phospholipase D proteins, PLDα1 and PLDγ1, at increased levels (supplemental Table 2). Recently, PLDα1-derived phosphatidic acid was shown to activate RBOHD-mediated reactive oxygen species production in response to ABA, and it is tempting to speculate that a similar mechanism could sustain reactive oxygen species production during ETI (62). Additionally, proteins with phospholipase A_2 activity (PLP2a/pPLA-IIα and SOBER1) increased significantly in PM fractions during ETI. PLP2a/pPLA-IIα has diverse lipid substrates *in vitro* and has been shown to accumulate during ETI and positively regulate cell death (41). In contrast, SOBER1 activity suppresses phosphatidic acid accumulation during ETI and represses HR in response to the effector AvrBsT (63). Thus, phospholipases with positive and negative roles in cell death accumulated at the PM during ETI, and lipid-derived signaling processes likely play a major role in the execution of ETI.

Membrane Trafficking—The trafficking of vesicles to and from the cell membrane is a key component of normal cellular function and plant-microbe interactions (21). Proteins involved in both endocytosis and exocytosis were up-regulated during ETI (supplemental Table 2). SNARE complexes are required for immune responses and are thought to function in the targeted exocytosis of various antimicrobial compounds and proteins (21, 64). We identified multiple SNARE complex constituents including the Syntaxin of plants 122 (SYP122), *N*-ethylmaleimide-sensitive factor vesicle fusing ATPase, and soluble *N*-ethylmaleimide-sensitive factor adaptor protein 33 (SNAP33) as highly increased at the PM during ETI (supplemental Table 2). Interestingly, despite the evidence that the closely related syntaxin PEN1/SYP121 has functionally specialized roles in innate immune responses, it was only moderately increased (~1.38-fold) at the PM during ETI, whereas SYP122 increased to much higher levels (~4.15-fold) (supplemental Table 1) (65). This observation suggests that SYP121 and SYP122 may have discrete functions in plant immunity depending on the immune recognition event.

Methionine Metabolism—Enzymes involved in the biosynthesis and recycling of methionine and *S*-adenosylmethionine (SAM) were identified at increased levels during ETI (supplemental Table 2). SAM is an important metabolic precursor for numerous bioactive compounds including the hormone ethylene (66). Up-regulation of methionine/SAM enzymes at the PM may provide the precursors for ethylene biosynthesis, which is known to be produced at high levels during the HR and is required for the acceleration of cell death (67). In support of this idea, the 1-aminocyclopropane-1-carboxylate oxidase ACO4/EFE, which catalyzes the final step of ethylene biosynthesis, was also found to be up-regulated at the PM (supplemental Table 2). SAM is a vital methyl group donor for methylation reactions in cellular metabolism (66). Several SAM-dependent methyltransferase enzymes were up-regulated at the PM during ETI, which suggests that SAM plays several roles during activation of plant immunity including the biosynthesis of the hormone ethylene and additional secondary metabolic processes (supplemental Table 2).

Protein Kinases/Phosphatases—Protein phosphorylation is a ubiquitous post-translational modification for the initiation and propagation of cellular signaling cascades. Many proteins involved in protein phosphorylation and dephosphorylation were significantly increased in the data set. Approximately 12% (35 of 286) of the proteins that were significantly up-regulated belong to the protein kinase superfamily. Receptor-like kinases (RLKs) and receptor-like cytoplasmic kinases represent the largest class of up-regulated kinases (supplemental Table 2). The DAMP RLK Pep1 receptor 1 (PEPR1) and Wall-associated kinase 1 (WAK1) were increased at the PM during ETI (supplemental Table 2) (2, 68). In addition, the receptor-like cytoplasmic kinase *Botrytis*-induced kinase 1 (BIK1), which is known to function in PTI responses to both the fungal necrotroph *Botrytis cinerea* and hemibiotroph bacterium *P. syringae*, was up-regulated at the PM during ETI (69). These data suggest that PTI-associated signaling processes are important components of ETI and that DAMP receptors may act to amplify immune signaling during execution of the HR.

Other RLKs involved in cell death regulation were also identified as up-regulated during ETI. Suppressor of BIR1 (SOBIR1), a positive regulator of cell death, increased at the PM. Five members of the cysteine-rich receptor kinase (CRK) family significantly increased (supplemental Table 2). Members of this family have been implicated in the activation of HR-like cell death and resistance to bacterial pathogens, and additional cysteine-rich receptor kinases may function in the execution of programmed cell death associated with plant immunity (70, 71). In addition to protein kinases, several protein phosphatase 2C family proteins were observed to increase during ETI (supplemental Table 2). Taken together, our results highlight the importance of protein kinase/phosphatase signaling during the execution of immune signaling.

Down-regulated Proteins and Processes—Because expression of the AvrRpt2 protease was used to initiate ETI signaling, it is expected that two classes of proteins would be detected at decreased levels in the data set: 1) proteins down-regulated by activation of ETI and 2) proteins directly cleaved by AvrRpt2. As expected, we identified RIN4 and other putative AvrRpt2 targets to be significantly decreased (supplemental Table 3). GO term biological processes enriched in the down-regulated protein set included photosynthesis, response to light, protein maturation, and receptor-mediated signaling (Fig. 4). Similar to the up-regulated protein set, there was a substantial proportion of RLKs that were down-regulated during ETI. However, multiple down-regulated RLKs have known roles in plant development, indicating that normal developmental processes are suspended during ETI.

AvrRpt2 Targets—RIN4 contains two AvrRpt2 recognition cleavage sites (amino acid sequence VP*x*FG*x*W) within a larger conserved nitrate-induced (NOI) domain (46, 72). In addition to RIN4, it has been hypothesized that AvrRpt2 has additional *in planta* physiological substrates when delivered into host cells (46, 72). Fourteen other *Arabidopsis* proteins share highly similar NOI/recognition cleavage site sequences and are predicted to localize to the PM (12, 72). However, evidence for AvrRpt2-mediated degradation of additional NOI proteins has been lacking in *Arabidopsis*. We robustly identified four additional NOI domain proteins, all of which change differentially (supplemental Tables 2 and 3). Of these, NOI4, NOI6, and NOI7 decrease to nearly undetectable levels in the presence of AvrRpt2, indicating that these proteins are likely *bona fide* AvrRpt2 targets in *Arabidopsis* (supplemental Table 3). Surprisingly, NOI10 was undetectable in control tissue but increased during ETI (supplemental Table 2). All of the observed peptides derived from NOI10 retained an intact recognition cleavage site, suggesting that this protein may not be an AvrRpt2 target in *Arabidopsis*. It is also possible that *NOI10* expression is highly induced during plant immune signaling and that the amount of AvrRpt2 in the GVG-AvrRpt2 plants is not enough to completely degrade NOI10. Previously it has been shown that NOI10 does not accumulate in the presence of AvrRpt2 in *Nicotiana benthamiana* transient expression assays, suggesting that it can be cleaved by AvrRpt2 (46). Thus, AvrRpt2 may exhibit differential specificity for NOI domain proteins in *Arabidopsis*, and native NOI10 may not be accessible to AvrRpt2.

Cytochrome P450s and Glucosinolate Metabolism—Cytochrome P450s (CYPs) represent a large family of enzymes with diverse substrates and are involved in various metabolic pathways. We identified 10 CYPs as decreasing in abundance during ETI, with at least two members present from each of the CYP71B, CYP706A, CYP83, and CYP89A subfamilies (supplemental Table 3). Of these, CYP83A1 and CYP83B1 are closely related but catalyze distinct steps in glucosinolate biosynthesis (73, 74). CYP83A1 substrates are primarily ali-

phatic aldoximes which are further processed into aliphatic glucosinolates, whereas CYP83B1 substrates are primarily aromatic aldoximes and are the precursors for indolic glucosinolates (73, 74). The complete absence of CYP83A1 and marked decrease in CP83B1 in PM-enriched fractions during ETI suggests that either glucosinolate production is greatly reduced or occurring elsewhere in the cell. Furthermore, the decrease in CYP83B1 and concomitant increase in camalexin biosynthetic enzymes suggests that indole-3-acetaldoxime (an important precursor in both pathways) is shuttled toward camalexin production, at the expense of indolic glucosinolates, during this stage of ETI (supplemental Tables 2 and 3).

Membrane Transport—Many enzymes involved in diverse membrane transport processes decreased at the PM during ETI including those involved in auxin, calcium, peptide, and sugar fluxes across the membrane (supplemental Table 3). Three enzymes that control auxin efflux were down-regulated at the PM. Auxin signaling can enhance plant susceptibility to *P. syringae*, and plants constitutively overexpressing AvrRpt2 exhibit altered auxin physiology through an unknown mechanism (75). It is unlikely that these auxin transporters are direct AvrRpt2 targets, but an indirect AvrRpt2 effect cannot be discounted (46, 75). Misregulated auxin transport has been shown to suppress systemic acquired resistance, immune-related hormone signaling, and the accumulation of various indolic metabolites including camalexin (76). Thus, it is possible that down-regulation of auxin efflux pumps is an important component of ETI-mediated systemic signaling and/or secondary metabolic processes.

Photosynthesis—The data set contains a moderate amount of proteins known to localize to chloroplasts and likely represents a source of contamination when performing two-phase partitioning from leaf tissue (supplemental Table 1). Interestingly, many proteins present on the thylakoid membrane appear to be decreased during ETI (supplemental Table 3). Chloroplast morphology and function is disrupted during execution of the HR, and it is likely the proteins that comprise the light harvesting complexes and reaction centers present on the thylakoid are degraded (77). It is also possible that thylakoid membrane surface properties change during ETI, disrupting its co-fractionation with PM vesicles during two-phase enrichment. Because many other chloroplast-localized proteins do not appear to change significantly in abundance (*e.g.* Rubisco), the protein complexes resident in the thylakoid might be specifically degraded during the onset of HR (supplemental Table 1).

Validation of Spectral Count Data—To confirm the spectral counting data as an accurate representation of protein levels in Col-0 WT and GVG-AvrRpt2 samples, we used immunoblotting as a complementary method to measure protein abundance changes during activation of ETI. Antibodies were obtained for six proteins that were differentially regulated in response to AvrRpt2, and immunoblots were performed on the same samples used for LC-MS/MS. Densitometric analysis of the resulting bands was conducted with ImageJ (Fig. 5 and supplemental Fig. 2). We were able to detect strong correlations between normalized spectral counts and immunoblot band intensity (Fig. 5). All of the Pearson correlation coefficients were high ($r > 0.88$, $p < 0.05$), indicating that both semiquantitative measurements (LC-MS/MS spectral counting and immunoblotting) are in agreement with regard to protein relative abundance between treatment and control samples.

Validation of Protein Level Changes during Pseudomonas Infection—To further validate the protein abundance changes observed in the LC-MS/MS data and to verify that these proteins are differentially regulated during bacterial infection, we monitored protein abundance changes during *Pst* DC3000 infection of *Arabidopsis*. Four-week-old Col-0 plants were vacuum-infiltrated with 10 mM $MgCl_2$, *Pst* DC3000 (*Pst* empty vector), or *Pst* DC3000 AvrRpt2 (*Pst* AvrRpt2). Under these infection conditions, HR was observed in plants infected with *Pst* AvrRpt2 ~16 h post-infiltration. PM vesicles were isolated 15 h post-infiltration. Immunoblots were performed on total leaf and PM-enriched fractions using the same antibodies as in Fig. 5. There was good correspondence between protein abundance changes observed in LC-MS/MS of GVG-AvrRpt2 transgenic plants and Col-0 WT plants infected with *Pst* AvrRpt2, indicating that the spectral counting data reflect biologically relevant protein regulation (Fig. 6). Many of the proteins tested also increased in abundance in response to *Pst* empty vector, albeit to a lesser extent than *Pst* AvrRpt2, suggesting that these proteins also play a role in plant basal immune responses.

Conclusion—Large scale quantitative proteomics studies of whole cell and subcellular-enriched fractions can elucidate global changes in protein abundance during diverse signaling events. This study represents the first large scale quantitative analysis of the plant plasma membrane proteome upon activation of an immune receptor. Because of the often observed disparities when comparing gene expression data and protein levels, quantitative proteomics represents a valuable means to more accurately assess (sub)cellular dynamics in response to diverse stimuli (78). Furthermore, we demonstrate that combining transgenic plant lines with inducible effector expression and quantitative MS/MS is a powerful tool for identifying proteins and processes that are targeted by individual effectors during infection.

The label-free spectral counting approach was found to be highly reproducible across multiple biological replicates, and protein abundance changes were confirmed during bacterial infection using immunoblotting (Table I and Figs. 5 and 6). Many proteins and processes were found to be differentially regulated during ETI, which demonstrates the dramatic modifications to cell physiology that occur during execution of plant immune responses. Significantly, a large percentage (>20%) of up-regulated proteins have known roles in plant defense or cell death, highlighting the importance of PM-

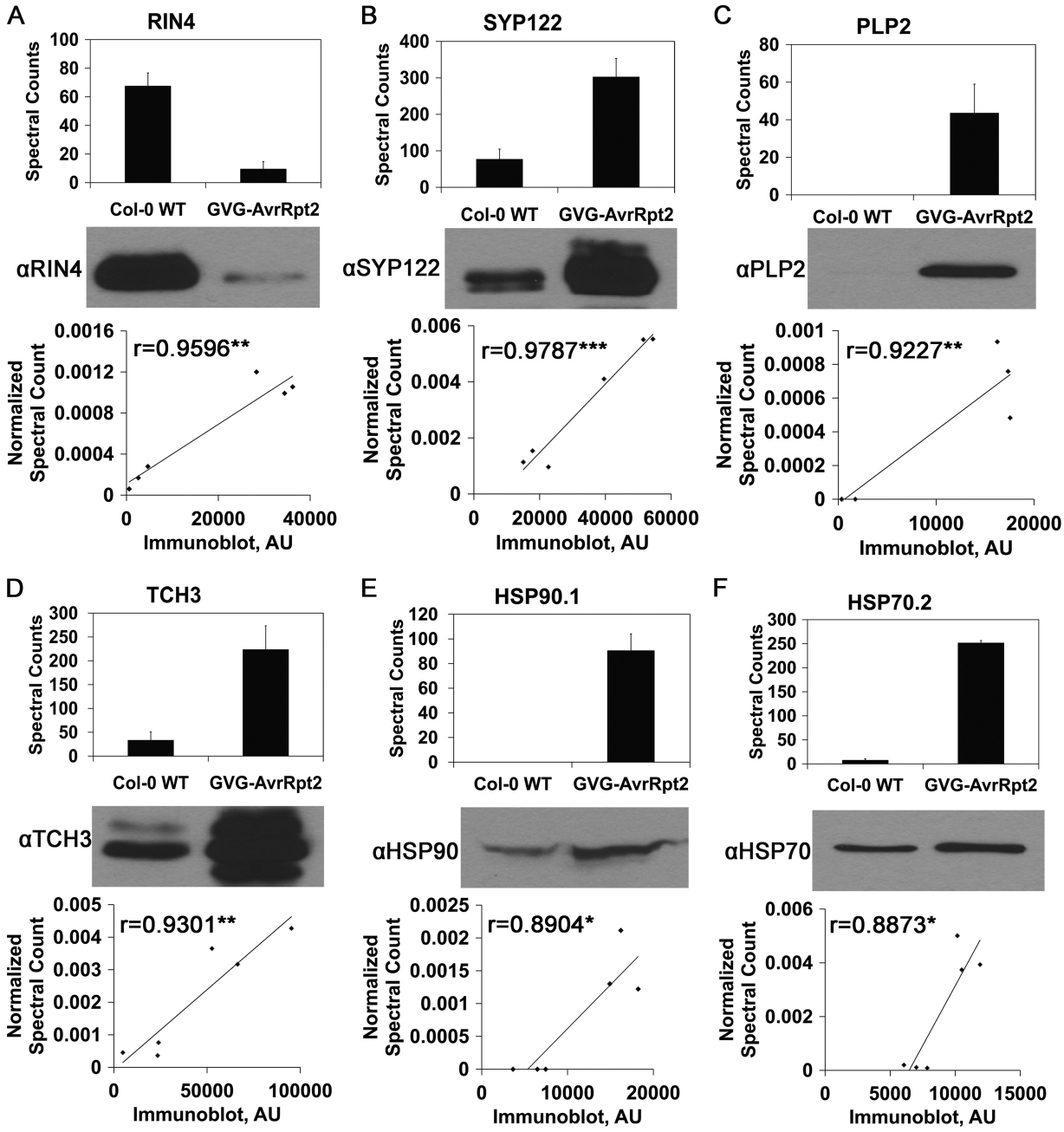

FIG. 5. **Protein spectral counts derived from MS/MS data correlate with immunoblot analysis.** *Top panels*, bar chart of raw spectral counts in Col-0 WT and GVG-AvrRpt2 samples. The values are the means ± S.D. *Middle panels*, representative immunoblot of Col-0 WT and GVG-AvrRpt2 PM-enriched fractions. *Bottom panels*, correlation of immunoblot band intensity and normalized spectral counts in each sample. The Pearson correlation coefficients (*r*) are reported. ***, $p < 0.001$; **, $p < 0.01$; *, $p < 0.05$. Immunoblot band density was measured in arbitrary units (*AU*). The HSP90 and HSP70 antibodies recognize multiple protein isoforms. *A*, RIN4. *B*, SYP122. *C*, PLP2a. *D*, TCH3. *E*, HSP90.1. *F*, HSP70.2.

associated immune signaling and defense responses. The identification of many known immune regulators provides *a posteriori* validation of our approach to identify novel components of immune signaling, and additional differentially regulated proteins represent exciting targets for future research.

The execution of ETI is a multilayered process that is often manifested as programmed cell death at sites of pathogen infection. Left unchecked, ETI has the potential to be deleterious, and therefore its activation and duration are tightly controlled. Under natural infection conditions, the HR is usually limited to one or a few cells via the attenuation of ETI responses. Plant mutants exhibiting defects in cell death control can exhibit uncontrolled, spreading lesions upon activation of ETI (79). Proteins involved in negative regulation of cell

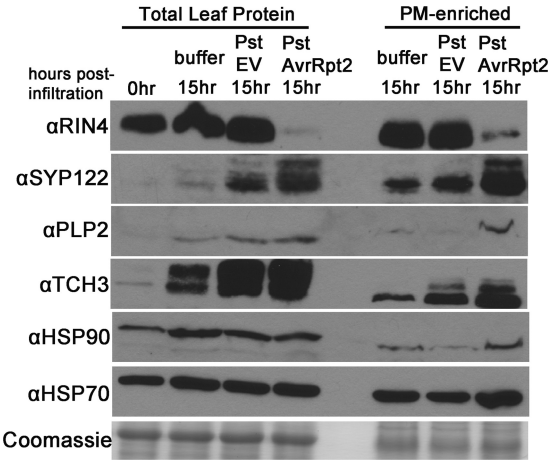

FIG. 6. **Spectral count data corresponds with protein changes during bacterial infection.** Levels of differentially regulated proteins in proteomics analysis change similarly during *P. syringae* pv. *tomato* strain DC3000 (*Pst*) infection of *Arabidopsis*. Col-0 plants were vacuum infiltrated with 10 mM $MgCl_2$ buffer, *Pst* expressing empty vector (*EV*), or *Pst* expressing AvrRpt2 at a concentration of 5×10^7 cfu/ml. The plants were harvested at 15 h post-infiltration and subjected to aqueous two-phase partitioning for PM enrichment. Total leaf and PM-enriched fractions were subjected to immunoblot analysis with the indicated protein antibodies. Coomassie staining indicates equal protein loading across samples. Total protein amounts for each blot are as follows: RIN4, total leaf protein: 20 μg, PM-enriched: 1 μg; SYP122, total leaf protein: 20 μg, PM-enriched: 1 μg; PLP2, 10 μg; TCH3, 5 μg; HSP90, 45 μg; HSP70, 10 μg; Coomassie gel, 10 μg.

death or defense responses, such as BIK1, BON1, RBOHD, RIPK, and SOBER1, increased in our study (supplemental Table 2) (12, 63, 80–85). The up-regulation of these immune signaling antagonists could reflect the repression of various immune processes to limit tissue damage. It is also possible that many proteins (*e.g.* BIK1, RIPK, or RBOHD) exhibit both positive and negative roles in defense signaling and cell death depending on complex interactions with other immune regulators, the stage of the immune response, and the pathogen assayed (12, 80–82). Ubiquitination and proteasome-mediated degradation of PTI and ETI receptors is emerging as an important regulatory mechanism to limit immune signaling, with degradation of the PTI receptor FLS2 occurring rapidly after activation by bacterial flagellin (17, 86). We identified many ubiquitin-related proteins and 26 S proteasome subunits as significantly increased during ETI, which might be involved in turnover of immune signaling components in addition to general protein catabolism during programmed cell death (supplemental Table 2). Dynamic interplay between positive and negative regulatory factors occurs during plant immunity, and together these signaling components are necessary for proper activation of plant immunity.

Understanding how changes in immune protein accumulation/function lead to effective disease resistance is a fundamental step toward engineering crops to be more resistant to pathogens. In this study, we were able to detect and quantify dynamic changes in the plasma membrane proteome upon activation of the RPS2 immune receptor. These data revealed a number of differentially regulated proteins whose role in immune signaling was previously unknown. Future large scale proteomic analyses of the overlap between PAMP and effector-triggered immune signaling at different times after elicitor treatment will facilitate a system-level understanding of plant innate immune signaling.

Acknowledgments—We thank the laboratories of B. Staskawicz, M. Boutry, K. Inoue, T. Ethlon, S. Dinesh-Kumar, B. Zolman, N. Raikhel, J. Braam, T. Heitz, and T. Nuhse for sharing antisera. We also thank Dr. Bryce Falk and Dr. George Bruening for the use of ultracentrifuges. We also thank Dr. Hyungwon Choi for helpful discussions regarding QSpec. The program for the distribution of nonunique peptide spectral counts was written by Nikhil Joshi at the University of California Davis Genome Center Bioinformatics Core Facility.

* This work was supported by National Science Foundation Grant MCB-1054298 and National Institutes of Health Grant RO1GM092772 (to G. C.). The costs of publication of this article were defrayed in part by the payment of page charges. This article must therefore be hereby marked "*advertisement*" in accordance with 18 U.S.C. Section 1734 solely to indicate this fact.

S This article contains supplemental material.

¶ Supported in part by National Science Foundation CREATE-IGERT Graduate Research Training Program Grant DGE-0653984.

** To whom correspondence should be addressed: Dept. of Plant Pathology, University of California, Davis, CA 95616. E-mail: glcoaker@ucdavis.edu.

Data availability: All raw data associated with this manuscript is available through the PeptideAtlas data repository using the following URL: http://www.peptideatlas.org/PASS/PASS00031

REFERENCES

1. Dodds, P. N., and Rathjen, J. P. (2010) Plant immunity: Towards an integrated view of plant-pathogen interactions. *Nat. Rev. Genet.* **11,** 539–548
2. Boller, T., and Felix, G. (2009) A renaissance of elicitors: Perception of microbe-associated molecular patterns and danger signals by pattern-recognition receptors. *Annu. Rev. Plant Biol.* **60,** 379–406
3. Block, A., and Alfano, J. R. (2011) Plant targets for *Pseudomonas syringae* type III effectors: Virulence targets or guarded decoys? *Curr. Opin. Microbiol.* **14,** 39–46
4. Mackey, D., Holt, B. F., 3rd, Wiig, A., and Dangl, J. L. (2002) RIN4 interacts with *Pseudomonas syringae* type III effector molecules and is required for RPM1-mediated resistance in *Arabidopsis*. *Cell* **108,** 743–754
5. Mackey, D., Belkhadir, Y., Alonso, J. M., Ecker, J. R., and Dangl, J. L. (2003) *Arabidopsis* RIN4 is a target of the type III virulence effector AvrRpt2 and modulates RPS2-mediated resistance. *Cell* **112,** 379–389
6. Axtell, M. J., and Staskawicz, B. J. (2003) Initiation of RPS2-specified disease resistance in *Arabidopsis* is coupled to the AvrRpt2-directed elimination of RIN4. *Cell* **112,** 369–377
7. Kim, M. G., da Cunha, L., McFall, A. J., Belkhadir, Y., DebRoy, S., Dangl, J. L., and Mackey, D. (2005) Two *Pseudomonas syringae* type III effectors inhibit RIN4-regulated basal defense in *Arabidopsis*. *Cell* **121,** 749–759
8. Liu, J., Elmore, J. M., Fuglsang, A. T., Palmgren, M. G., Staskawicz, B. J., and Coaker, G. (2009) RIN4 functions with the plasma membrane H^+-ATPase to regulate stomatal apertures during pathogen attack. *PLoS Biol.* **7,** e1000139
9. Nimchuk, Z., Marois, E., Kjemtrup, S., Leister, R. T., Katagiri, F., and Dangl, J. L. (2000) Eukaryotic fatty acylation drives plasma membrane targeting and enhances function of several type III effector proteins from *Pseudomonas syringae*. *Cell* **101,** 353–363
10. Wilton, M., Subramaniam, R., Elmore, J., Felsensteiner, C., Coaker, G., and Desveaux, D. (2010) The type III effector HopF2Pto targets *Arabidopsis*

RIN4 protein to promote *Pseudomonas syringae* virulence. *Proc. Natl. Acad. Sci. U.S.A.* **107,** 2349–2354
11. Chung, E. H., da Cunha, L., Wu, A. J., Gao, Z., Cherkis, K., Afzal, A. J., Mackey, D., and Dangl, J. L. (2011) Specific threonine phosphorylation of a host target by two unrelated type III effectors activates a host innate immune receptor in plants. *Cell Host Microbe* **9,** 125–136
12. Liu, J., Elmore, J. M., Lin, Z. J., and Coaker, G. (2011) A receptor-like cytoplasmic kinase phosphorylates the host target RIN4, leading to the activation of a plant innate immune receptor. *Cell Host Microbe* **9,** 137–146
13. Tsuda, K., and Katagiri, F. (2010) Comparing signaling mechanisms engaged in pattern-triggered and effector-triggered immunity. *Curr. Opin. Plant Biol.* **13,** 459–465
14. Nühse, T. S., Bottrill, A. R., Jones, A. M., and Peck, S. C. (2007) Quantitative phosphoproteomic analysis of plasma membrane proteins reveals regulatory mechanisms of plant innate immune responses. *Plant J.* **51,** 931–940
15. Benschop, J. J., Mohammed, S., O'Flaherty, M., Heck, A. J., Slijper, M., and Menke, F. L. (2007) Quantitative phosphoproteomics of early elicitor signaling in *Arabidopsis*. *Mol. Cell. Proteomics* **6,** 1198–1214
16. Keinath, N. F., Kierszniowska, S., Lorek, J., Bourdais, G., Kessler, S. A., Shimosato-Asano, H., Grossniklaus, U., Schulze, W. X., Robatzek, S., and Panstruga, R. (2010) PAMP (pathogen-associated molecular pattern)-induced changes in plasma membrane compartmentalization reveal novel components of plant immunity. *J. Biol. Chem.* **285,** 39140–39149
17. Lu, D., Lin, W., Gao, X., Wu, S., Cheng, C., Avila, J., Heese, A., Devarenne, T. P., He, P., and Shan, L. (2011) Direct ubiquitination of pattern recognition receptor FLS2 attenuates plant innate immunity. *Science* **332,** 1439–1442
18. Jones, A. M., Thomas, V., Truman, B., Lilley, K., Mansfield, J., and Grant, M. (2004) Specific changes in the *Arabidopsis* proteome in response to bacterial challenge: Differentiating basal and R-gene mediated resistance. *Phytochemistry* **65,** 1805–1816
19. Widjaja, I., Naumann, K., Roth, U., Wolf, N., Mackey, D., Dangl, J. L., Scheel, D., and Lee, J. (2009) Combining subproteome enrichment and Rubisco depletion enables identification of low abundance proteins differentially regulated during plant defense. *Proteomics* **9,** 138–147
20. Caplan, J. L., Zhu, X., Mamillapalli, P., Marathe, R., Anandalakshmi, R., and Dinesh-Kumar, S. P. (2009) Induced ER chaperones regulate a receptor-like kinase to mediate antiviral innate immune response in plants. *Cell Host Microbe* **6,** 457–469
21. Bednarek, P., Kwon, C., and Schulze-Lefert, P. (2010) Not a peripheral issue: Secretion in plant-microbe interactions. *Curr. Opin. Plant Biol.* **13,** 378–387
22. Hatsugai, N., Iwasaki, S., Tamura, K., Kondo, M., Fuji, K., Ogasawara, K., Nishimura, M., and Hara-Nishimura, I. (2009) A novel membrane fusion-mediated plant immunity against bacterial pathogens. *Genes Dev.* **23,** 2496–2506
23. McNellis, T. W., Mudgett, M. B., Li, K., Aoyama, T., Horvath, D., Chua, N. H., and Staskawicz, B. J. (1998) Glucocorticoid-inducible expression of a bacterial avirulence gene in transgenic *Arabidopsis* induces hypersensitive cell death. *Plant J.* **14,** 247–257
24. Larsson, C., Sommarin, M., Widell, S., and Harry Walter and Gote, J. (1994) Isolation of highly purified plant plasma membranes and separation of inside-out and right-side-out vesicles. *Methods Enzymol.* Vol. 228, 451–469
25. Johansson, F., Olbe, M., Sommarin, M., and Larsson, C. (1995) Brij 58, a polyoxyethylene acyl ether, creates membrane vesicles of uniform sidedness: A new tool to obtain inside-out (cytoplasmic side-out) plasma membrane vesicles. *Plant J.* **7,** 165–173
26. Wessel, D., and Flügge, U. I. (1984) A method for the quantitative recovery of protein in dilute solution in the presence of detergents and lipids. *Anal. Biochem.* **138,** 141–143
27. Laemmli, U. K. (1970) Cleavage of structural proteins during the assembly of the head of bacteriophage T4. *Nature* **227,** 680–685
28. Shevchenko, A., Tomas, H., Havlis, J., Olsen, J. V., and Mann, M. (2006) In-gel digestion for mass spectrometric characterization of proteins and proteomes. *Nat. Protoc.* **1,** 2856–2860
29. Alvarado, R., Tran, D., Ching, B., and Phinney, B. S. (2010) A comparative study of in-gel digestions using microwave and pressure-accelerated technologies. *J. Biomol. Tech.* **21,** 148–155
30. Craig, R., and Beavis, R. C. (2004) TANDEM: Matching proteins with tandem mass spectra. *Bioinformatics* **20,** 1466–1467
31. Käll, L., Storey, J. D., MacCoss, M. J., and Noble, W. S. (2008) Assigning significance to peptides identified by tandem mass spectrometry using decoy databases. *J. Proteome Res.* **7,** 29–34
32. Keller, A., Nesvizhskii, A. I., Kolker, E., and Aebersold, R. (2002) Empirical statistical model to estimate the accuracy of peptide identifications made by MS/MS and database search. *Anal. Chem.* **74,** 5383–5392
33. Zhang, Y., Wen, Z., Washburn, M. P., and Florens, L. (2010) Refinements to label free proteome quantitation: How to deal with peptides shared by multiple proteins. *Anal. Chem.* **82,** 2272–2281
34. Liao, Y., Alvarado, R., Phinney, B., and Lönnerdal, B. (2011) Proteomic characterization of human milk whey proteins during a twelve-month lactation period. *J. Proteome Res.* **10,** 1746–1754
35. Choi, H., Fermin, D., and Nesvizhskii, A. I. (2008) Significance analysis of spectral count data in label-free shotgun proteomics. *Mol. Cell. Proteomics* **7,** 2373–2385
36. Huang, da W., Sherman, B. T., and Lempicki, R. A. (2009) Systematic and integrative analysis of large gene lists using DAVID bioinformatics resources. *Nat. Protoc.* **4,** 44–57
37. Morsomme, P., Dambly, S., Maudoux, O., and Boutry, M. (1998) Single point mutations distributed in 10 soluble and membrane regions of the Nicotiana plumbaginifolia plasma membrane PMA2 H^+-ATPase activate the enzyme and modify the structure of the C-terminal region. *J. Biol. Chem.* **273,** 34837–34842
38. Dávila-Aponte, J. A., Inoue, K., and Keegstra, K. (2003) Two chloroplastic protein translocation components, Tic110 and Toc75, are conserved in different plastid types from multiple plant species. *Plant Mol. Biol.* **51,** 175–181
39. Lingard, M. J., Monroe-Augustus, M., and Bartel, B. (2009) Peroxisome-associated matrix protein degradation in *Arabidopsis*. *Proc. Natl. Acad. Sci. U.S.A.* **106,** 4561–4566
40. Antosiewicz, D. M., Polisensky, D. H., and Braam, J. (1995) Cellular localization of the Ca^{2+} binding TCH3 protein of *Arabidopsis*. *Plant J.* **8,** 623–636
41. La Camera, S., Geoffroy, P., Samaha, H., Ndiaye, A., Rahim, G., Legrand, M., and Heitz, T. (2005) A pathogen-inducible patatin-like lipid acyl hydrolase facilitates fungal and bacterial host colonization in *Arabidopsis*. *Plant J.* **44,** 810–825
42. Nühse, T. S., Boller, T., and Peck, S. C. (2003) A plasma membrane syntaxin is phosphorylated in response to the bacterial elicitor flagellin. *J. Biol. Chem.* **278,** 45248–45254
43. Gassmann, M., Grenacher, B., Rohde, B., and Vogel, J. (2009) Quantifying Western blots: Pitfalls of densitometry. *Electrophoresis* **30,** 1845–1855
44. Kunkel, B. N., Bent, A. F., Dahlbeck, D., Innes, R. W., and Staskawicz, B. J. (1993) RPS2, an *Arabidopsis* disease resistance locus specifying recognition of *Pseudomonas syringae* strains expressing the avirulence gene avrRpt2. *Plant Cell* **5,** 865–875
45. Coaker, G., Falick, A., and Staskawicz, B. (2005) Activation of a phytopathogenic bacterial effector protein by a eukaryotic cyclophilin. *Science* **308,** 548–550
46. Chisholm, S. T., Dahlbeck, D., Krishnamurthy, N., Day, B., Sjolander, K., and Staskawicz, B. J. (2005) Molecular characterization of proteolytic cleavage sites of the *Pseudomonas syringae* effector AvrRpt2. *Proc. Natl. Acad. Sci. U.S.A.* **102,** 2087–2092
47. Larsson, C., Widell, S., and Kjellbom, P. (1987) Preparation of high-purity plasma membranes. *Methods Enzymol.* Vol. 148, 558–568
48. Heazlewood, J. L., Verboom, R. E., Tonti-Filippini, J., Small, I., and Millar, A. H. (2007) SUBA: The *Arabidopsis* Subcellular Database. *Nucleic Acids Res.* **35,** D213–D218
49. Nelson, C. J., Hegeman, A. D., Harms, A. C., and Sussman, M. R. (2006) A quantitative analysis of *Arabidopsis* plasma membrane using trypsin-catalyzed ^{18}O labeling. *Mol. Cell. Proteomics* **5,** 1382–1395
50. Lundgren, D. H., Hwang, S. I., Wu, L., and Han, D. K. (2010) Role of spectral counting in quantitative proteomics. *Expert Rev. Proteomics* **7,** 39–53
51. Liu, H., Sadygov, R. G., and Yates, J. R., 3rd (2004) A model for random sampling and estimation of relative protein abundance in shotgun proteomics. *Anal. Chem.* **76,** 4193–4201
52. De Michele, R., Vurro, E., Rigo, C., Costa, A., Elviri, L., Di Valentin, M., Careri, M., Zottini, M., Sanità di Toppi, L., and Lo Schiavo, F. (2009) Nitric

oxide is involved in cadmium-induced programmed cell death in *Arabidopsis* suspension cultures. *Plant Physiol.* **150,** 217–228
53. Bolton, M. D. (2009) Primary metabolism and plant defense: Fuel for the fire. *Mol. Plant-Microbe Interact.* **22,** 487–497
54. Tsuji, J., Jackson, E. P., Gage, D. A., Hammerschmidt, R., and Somerville, S. C. (1992) Phytoalexin accumulation in *Arabidopsis thaliana* during the hypersensitive reaction to *Pseudomonas syringae* pv syringae. *Plant Physiol.* **98,** 1304–1309
55. Schuhegger, R., Nafisi, M., Mansourova, M., Petersen, B. L., Olsen, C. E., Svatos, A., Halkier, B. A., and Glawischnig, E. (2006) CYP71B15 (PAD3) catalyzes the final step in camalexin biosynthesis. *Plant Physiol.* **141,** 1248–1254
56. Millet, Y. A., Danna, C. H., Clay, N. K., Songnuan, W., Simon, M. D., Werck-Reichhart, D., and Ausubel, F. M. (2010) Innate immune responses activated in *Arabidopsis* roots by microbe-associated molecular patterns. *Plant Cell* **22,** 973–990
57. Nafisi, M., Goregaoker, S., Botanga, C. J., Glawischnig, E., Olsen, C. E., Halkier, B. A., and Glazebrook, J. (2007) *Arabidopsis* cytochrome P450 monooxygenase 71A13 catalyzes the conversion of indole-3-acetaldoxime in camalexin synthesis. *Plant Cell* **19,** 2039–2052
58. Su, T., Xu, J., Li, Y., Lei, L., Zhao, L., Yang, H., Feng, J., Liu, G., and Ren, D. (2011) Glutathione-indole-3-acetonitrile is required for camalexin biosynthesis in *Arabidopsis thaliana*. *Plant Cell* **23,** 364–380
59. Glawischnig, E. (2007) Camalexin. *Phytochemistry* **68,** 401–406
60. Wang, X. (2004) Lipid signaling. *Curr. Opin. Plant Biol.* **7,** 329–336
61. Andersson, M. X., Kourtchenko, O., Dangl, J. L., Mackey, D., and Ellerström, M. (2006) Phospholipase-dependent signalling during the AvrRpm1- and AvrRpt2-induced disease resistance responses in *Arabidopsis thaliana*. *Plant J.* **47,** 947–959
62. Zhang, Y., Zhu, H., Zhang, Q., Li, M., Yan, M., Wang, R., Wang, L., Welti, R., Zhang, W., and Wang, X. (2009) Phospholipase Dα1 and phosphatidic acid regulate NADPH oxidase activity and production of reactive oxygen species in ABA-mediated stomatal closure in *Arabidopsis*. *Plant Cell* **21,** 2357–2377
63. Kirik, A., and Mudgett, M. B. (2009) SOBER1 phospholipase activity suppresses phosphatidic acid accumulation and plant immunity in response to bacterial effector AvrBsT. *Proc. Natl. Acad. Sci. U.S.A.* **106,** 20532–20537
64. Kwon, C., Neu, C., Pajonk, S., Yun, H. S., Lipka, U., Humphry, M., Bau, S., Straus, M., Kwaaitaal, M., Rampelt, H., El Kasmi, F., Jürgens, G., Parker, J., Panstruga, R., Lipka, V., and Schulze-Lefert, P. (2008) Co-option of a default secretory pathway for plant immune responses. *Nature* **451,** 835–840
65. Pajonk, S., Kwon, C., Clemens, N., Panstruga, R., and Schulze-Lefert, P. (2008) Activity determinants and functional specialization of *Arabidopsis* PEN1 syntaxin in innate immunity. *J. Biol. Chem.* **283,** 26974–26984
66. Roje, S. (2006) *S*-Adenosyl-L-methionine: Beyond the universal methyl group donor. *Phytochemistry* **67,** 1686–1698
67. Liu, H., Wang, Y., Xu, J., Su, T., Liu, G., and Ren, D. (2008) Ethylene signaling is required for the acceleration of cell death induced by the activation of AtMEK5 in *Arabidopsis*. *Cell Res.* **18,** 422–432
68. Brutus, A., Sicilia, F., Macone, A., Cervone, F., and De Lorenzo, G. (2010) A domain swap approach reveals a role of the plant wall-associated kinase 1 (WAK1) as a receptor of oligogalacturonides. *Proc. Natl. Acad. Sci. U.S.A.* **107,** 9452–9457
69. Laluk, K., Luo, H., Chai, M., Dhawan, R., Lai, Z., and Mengiste, T. (2011) Biochemical and genetic requirements for function of the immune response regulator BOTRYTIS-INDUCED KINASE1 in plant growth, ethylene signaling, and PAMP-triggered immunity in *Arabidopsis*. *Plant Cell* Vol. 23, 2831–2849
70. Chen, K., Fan, B., Du, L., and Chen, Z. (2004) Activation of hypersensitive cell death by pathogen-induced receptor-like protein kinases from *Arabidopsis*. *Plant Mol. Biol.* **56,** 271–283
71. Acharya, B. R., Raina, S., Maqbool, S. B., Jagadeeswaran, G., Mosher, S. L., Appel, H. M., Schultz, J. C., Klessig, D. F., and Raina, R. (2007) Overexpression of CRK13, an *Arabidopsis* cysteine-rich receptor-like kinase, results in enhanced resistance to *Pseudomonas syringae*. *Plant J.* **50,** 488–499
72. Kim, H. S., Desveaux, D., Singer, A. U., Patel, P., Sondek, J., and Dangl, J. L. (2005) The *Pseudomonas syringae* effector AvrRpt2 cleaves its C-terminally acylated target, RIN4, from *Arabidopsis* membranes to block RPM1 activation. *Proc. Natl. Acad. Sci. U.S.A.* **102,** 6496–6501
73. Bak, S., and Feyereisen, R. (2001) The involvement of two P450 enzymes, CYP83B1 and CYP83A1, in auxin homeostasis and glucosinolate biosynthesis. *Plant Physiol.* **127,** 108–118
74. Naur, P., Petersen, B. L., Mikkelsen, M. D., Bak, S., Rasmussen, H., Olsen, C. E., and Halkier, B. A. (2003) CYP83A1 and CYP83B1, Two nonredundant cytochrome P450 enzymes metabolizing oximes in the biosynthesis of glucosinolates in *Arabidopsis*. *Plant Physiol.* **133,** 63–72
75. Chen, Z., Agnew, J. L., Cohen, J. D., He, P., Shan, L., Sheen, J., and Kunkel, B. N. (2007) *Pseudomonas syringae* type III effector AvrRpt2 alters *Arabidopsis thaliana* auxin physiology. *Proc. Natl. Acad. Sci. U.S.A.* **104,** 20131–20136
76. Truman, W. M., Bennett, M. H., Turnbull, C. G., and Grant, M. R. (2010) *Arabidopsis* auxin mutants are compromised in systemic acquired resistance and exhibit aberrant accumulation of various indolic compounds. *Plant Physiol.* **152,** 1562–1573
77. Mur, L. A., Kenton, P., Lloyd, A. J., Ougham, H., and Prats, E. (2008) The hypersensitive response: The centenary is upon us but how much do we know? *J. Exp. Bot.* **59,** 501–520
78. Fu, X., Fu, N., Guo, S., Yan, Z., Xu, Y., Hu, H., Menzel, C., Chen, W., Li, Y., Zeng, R., and Khaitovich, P. (2009) Estimating accuracy of RNA-Seq and microarrays with proteomics. *BMC Genomics* **10,** 161
79. Lorrain, S., Vailleau, F., Balagué, C., and Roby, D. (2003) Lesion mimic mutants: Keys for deciphering cell death and defense pathways in plants? *Trends Plant Sci.* **8,** 263–271
80. Veronese, P., Nakagami, H., Bluhm, B., Abuqamar, S., Chen, X., Salmeron, J., Dietrich, R. A., Hirt, H., and Mengiste, T. (2006) The membrane-anchored BOTRYTIS-INDUCED KINASE1 plays distinct roles in *Arabidopsis* resistance to necrotrophic and biotrophic pathogens. *Plant Cell* **18,** 257–273
81. Pogány, M., von Rad, U., Grün, S., Dongó, A., Pintye, A., Simoneau, P., Bahnweg, G., Kiss, L., Barna, B., and Durner, J. (2009) Dual roles of reactive oxygen species and NADPH oxidase RBOHD in an *Arabidopsis*-alternaria pathosystem. *Plant Physiol.* **151,** 1459–1475
82. Torres, M. A., Jones, J. D., and Dangl, J. L. (2005) Pathogen-induced, NADPH oxidase-derived reactive oxygen intermediates suppress spread of cell death in *Arabidopsis thaliana*. *Nat. Genet.* **37,** 1130–1134
83. Gao, M., Wang, X., Wang, D., Xu, F., Ding, X., Zhang, Z., Bi, D., Cheng, Y. T., Chen, S., Li, X., and Zhang, Y. (2009) Regulation of cell death and innate immunity by two receptor-like kinases in *Arabidopsis*. *Cell Host Microbe* **6,** 34–44
84. Jambunathan, N., Siani, J. M., and McNellis, T. W. (2001) A humidity-sensitive *Arabidopsis* copine mutant exhibits precocious cell death and increased disease resistance. *Plant Cell* **13,** 2225–2240
85. Yang, S., Yang, H., Grisafi, P., Sanchatjate, S., Fink, G. R., Sun, Q., and Hua, J. (2006) The BON/CPN gene family represses cell death and promotes cell growth in *Arabidopsis*. *Plant J.* **45,** 166–179
86. Cheng, Y. T., Li, Y., Huang, S., Huang, Y., Dong, X., Zhang, Y., and Li, X. (2011) Stability of plant immune-receptor resistance proteins is controlled by SKP1-CULLIN1-F-box (SCF)-mediated protein degradation. *Proc. Natl. Acad. Sci. U.S.A.* Vol. 108, 14694–14699